THE JOURNAL OF BIOLOGICAL CHEMISTRY
Vol. 273, No. 44, Issue of October 30, pp. 28994–29001, 1998

Printed in U.S.A.

When Size Is Important

ACCOMMODATION OF MAGNESIUM IN A CALCIUM BINDING REGULATORY DOMAIN*

(Received for publication, June 29, 1998, and in revised form, August 10, 1998)

Anders Malmendal‡, Johan Evenäs, Eva Thulin, Garry P. Gippert, Torbjörn Drakenberg, and Sture Forsén

From Physical Chemistry 2, Lund University, P.O. Box 124, S-22100 Lund, Sweden

The accommodation of Mg^{2+} in the N-terminal domain of calmodulin was followed through amide ^{1}H and ^{15}N chemical shifts and line widths in heteronuclear single-quantum coherence spectroscopy NMR spectra. Mg^{2+} binds sequentially to the two Ca^{2+}-binding loops in this domain, with affinities such that nearly half of the loops would be occupied by Mg^{2+} in resting eukaryotic cells. Mg^{2+} binding seems to occur without ligation to the residue in the 12th loop position, previously proven largely responsible for the major rearrangements induced by binding of the larger Ca^{2+}. Consequently, smaller Mg^{2+}-induced structural changes are indicated throughout the protein. The two Ca^{2+}-binding loops have different Mg^{2+} binding characteristics. Ligands in the N-terminal loop I are better positioned for cation binding, resulting in higher affinity and slower binding kinetics compared with the C-terminal loop II (k_{off} = 380 ± 40 s^{-1} compared with ~10,000 s^{-1} at 25 °C). The Mg^{2+}-saturated loop II undergoes conformational exchange on the 100-μs time scale. Available data suggest that this exchange occurs between a conformation providing a ligand geometry optimized for Mg^{2+} binding and a conformation more similar to that of the empty loop.

Mg^{2+} is an essential ion in biological systems, with structural and catalytic functions (1, 2). It is the most abundant divalent metal ion in mammalian cells, with the cytosolic free concentration kept nearly constant at 0.5–2.0 mM (3). In this milieu, Ca^{2+} is able to regulate a vast number of cellular activities through transient increases in cytosolic concentration from less than 0.1 μM in a resting cell to 1–10 μM in an activated cell (4). Thus, the primary protein targets of Ca^{2+}, in many cases calmodulin (CaM)[1] or other EF-hand proteins, must be able to respond in a 100–10,000-fold excess of Mg^{2+}. Due to the high abundance of Mg^{2+}, intracellular Mg^{2+}-specific proteins need no structural discrimination against Ca^{2+} (5). In contrast, Ca^{2+}-binding proteins may accomplish discrimination against Mg^{2+} by taking advantage of the larger ionic radius of Ca^{2+} and its less stringent demands on the number (often 6–8) and spatial arrangement of coordinating oxygen ligands, as compared with Mg^{2+}, which has a strong preference for 6-fold coordination in an octahedral symmetry (6, 7). For example, the Mg^{2+} affinities of the two sites in toad parvalbumin are about a factor of 6000 lower than the Ca^{2+} affinities (8). However, the high cytosolic Mg^{2+} concentration implies that many Ca^{2+} sites are occupied by Mg^{2+} in resting cells.

The EF-hand family of Ca^{2+}-binding proteins may be divided into distinct subfamilies, *e.g.* CaM, troponin C, parvalbumins, and S100 proteins (9). In these proteins, Ca^{2+} binds in the loop region of a 29-residue-long EF-hand helix-loop-helix motif (10). This motif, which is among the five most common protein motifs in animal cells (11), usually appears in pairs, where cooperative Ca^{2+} binding frequently is observed (7). The consensus EF-hand loop comprises 12 residues arranged to coordinate the Ca^{2+} with pentagonal bipyramid symmetry, with the seven ligands provided by five side chain carboxylate oxygens, one backbone carbonyl oxygen, and one water oxygen (12). Two of the side chain ligands are provided by a conserved, bidentate Glu in the 12th and last loop position (Fig. 1*a*).

Calmodulin, the ubiquitous regulatory Ca^{2+}-binding protein in eukaryotic cells, consists of two distinct domains connected by a flexible tether. The two domains are structurally similar, and each has two EF-hands packed in a roughly parallel fashion with a short β-sheet connecting the Ca^{2+}-binding loops (Fig. 1). The eight helices and four binding loops are denoted A–H and I–IV, respectively. Within each domain, the two EF-hands are connected by a short linker, *i.e.* between helices B and C and between F and G. Each domain binds two Ca^{2+} with positive cooperativity (13, 14). Upon Ca^{2+} binding, the secondary structure in both domains remains essentially unchanged, while the relative orientations of the helices change in such a way that the domains go from a relatively compact, "closed" structure (Fig. 1*b*) to an "open" structure with well defined hydrophobic patches where target proteins may bind (Fig. 1*c*) (15–19). The two domains of CaM can be expressed and produced independently (20), fold independently (18, 21), and have Ca^{2+} binding characteristics similar to intact CaM (13). These protein "fragments" were originally produced by trypsin cleavage of CaM in presence of Ca^{2+} and are named TR_1C and TR_2C, respectively (22, 23).

The Mg^{2+} dissociation constants of CaM are in the millimolar range (24, 25), and Mg^{2+} has generally been assumed to bind to the same sites as Ca^{2+} (25, 26) but to induce only small structural rearrangements (24, 26). This was recently verified by Ohki *et al.* using ^{1}H–^{15}N NMR (27). The Mg^{2+}-loaded form of CaM is reported to cause only negligible activation of CaM

* This research was supported by Swedish Natural Science Research Council Grant K-AA/KU 02545-326. The 600-MHz spectrometer was purchased by a grant from the Knut and Alice Wallenberg Foundation. The costs of publication of this article were defrayed in part by the payment of page charges. This article must therefore be hereby marked "*advertisement*" in accordance with 18 U.S.C. Section 1734 solely to indicate this fact.

‡ To whom correspondence should be addressed. Tel.: 46-46-222-8207; Fax: 46–46-222-4543; E-mail: anders@bor.fkem2.lth.se.

[1] The abbreviations used are: CaM, calmodulin; helix A, residues 6–20; helix B, residues 29–38; helix C, residues 45–56; helix D, residues 65–75; HSQC, heteronuclear single-quantum coherence spectroscopy; K_1, first macroscopic binding constant; K_2, second macroscopic binding constant; K_I, microscopic binding constant of loop I; K_{II}, microscopic binding constant of loop II; k_{off}, off-rate; k_{on}, on-rate; linker, residues 39–44; loop I, residues 20–31; loop II, residues 56–67; NOESY, nuclear Overhauser effect spectroscopy; TOCSY, total correlation spectroscopy; TR_1C, the recombinant N-terminal domain of calmodulin (Ala^1–Asp^{80}) with an additional N-terminal Met; TR_2C, the recombinant C-terminal domain of calmodulin (Met^{76}–Lys^{148}).

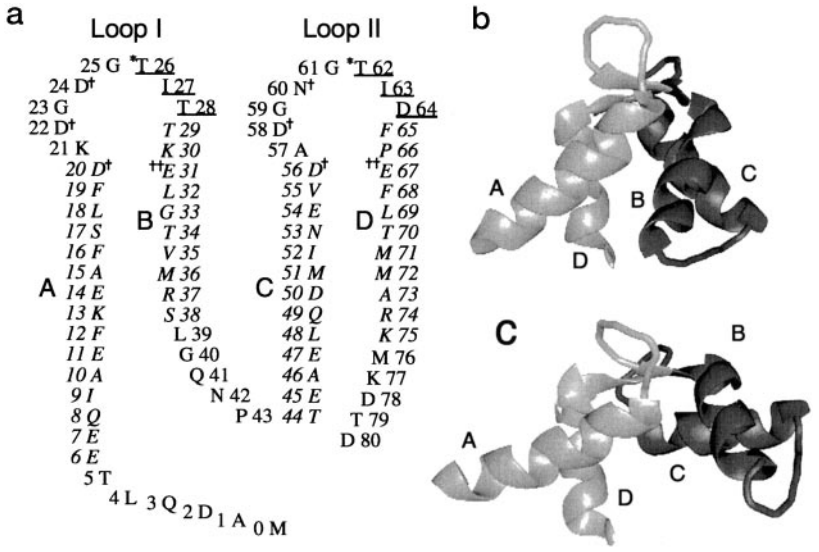

FIG. 1. **Amino acid sequence and secondary structure (*a*), and three-dimensional structures of the "closed" ion-free (16) (*b*) and "open" Ca^{2+}-loaded (15) (*c*) states of the N-terminal domain of calmodulin.** *a*, the one-letter codes for amino acid residues are used. The ion-free TR_1C secondary structure (16) is indicated with helical residues in *italic type* and β-sheet residues *underlined*. Ca^{2+} coordination is indicated as follows: main chain carbonyl oxygens (*asterisks*), monodentate carboxylates (*single daggers*), and bidentate carboxylates (*double daggers*). The helices are denoted A–D. *b* and *c*, residues Thr^5–Ile^{27} and Ile^{63}–Lys^{75} are shown in *light gray*, and Thr^{28}–Thr^{62} are *dark gray*. The β-strands (Thr^{26}–Thr^{28}, Thr^{62}–Asp^{64}) are oriented similarly in the two structures. This *figure* was generated using UCSF software Midas Plus (60).

target proteins (28, 29). At the time of writing, x-ray structures of Mg^{2+}-loaded EF-hand sites are only available for pike parvalbumin (30), myosin regulatory light chain (31), and calbindin D_{9k} (32). In parvalbumin and myosin regulatory light chain, the only difference between Mg^{2+} and Ca^{2+} ligation is that the residues in the 12th loop positions serve as monodentate ligands in the Mg^{2+} structures but bidentate in the Ca^{2+} structures. In calbindin D_{9k}, the Glu in the 12th position is not used for direct Mg^{2+} ligation. Instead, a water molecule is inserted between the side chain and Mg^{2+}. The Glu in the 12th loop position has been shown to be very important for the structural rearrangements from a "closed" to an "open" conformation occurring upon Ca^{2+} binding (33–35).

In the present study, the TR_1C fragment of vertebrate CaM was titrated by Mg^{2+} and followed by ^1H–^{15}N NMR, in order to address the questions regarding the detailed Mg^{2+} binding characteristics of this CaM domain and the structural and dynamic nature of protein states at different levels of Mg^{2+} saturation.

EXPERIMENTAL PROCEDURES

Protein Synthesis—The synthetic gene for TR_1C was constructed from overlapping oligonucleotides,[2] essentially as described for calbindin D_{9k} (36). The TR_1C gene was cloned into the pRCB1 plasmid. Unlabeled and uniformly ^{15}N-labeled TR_1C was expressed in *Escherichia coli* and purified as reported previously for the TR_2C fragment (18).

NMR Experimental Parameters—^1H and ^{15}N chemical shifts of $(Mg^{2+})_2$-TR_1C were assigned at 25 °C, pH 7.2, on 4 mM protein samples of unlabeled and ^{15}N-labeled TR_1C in H_2O with 10% D_2O, 30 mM $MgCl_2$, 10 mM KCl, and 100 μM NaN_3. The assignments were obtained from COSY (37), R-COSY (38 ms) (38), 2Q (30 ms) (39), TOCSY (110 ms) (40, 41) with DIPSI-2rc mixing (42), and NOESY (120 ms) (43) spectra acquired on the unlabeled sample. Sensitivity-enhanced and gradient-selected (44) two-dimensional ^{15}N HSQC-TOCSY with DIPSI-2rc mixing (110 ms) and three-dimensional ^{15}N NOESY-HSQC (150 ms) spectra were acquired on the ^{15}N-labeled sample. Water was suppressed by weak presaturation (1.3 s) in the ^1H NMR experiments, and by water-flip-back pulses (45) in the ^1H-^{15}N experiments.

The $MgCl_2$ titration on TR_1C monitored by ^1H-^{15}N HSQC was performed at 25 °C, pH 7.5, on a 0.46 mM ^{15}N-labeled TR_1C sample in H_2O with 10% D_2O, 150 mM KCl, 100 μM NaN_3, and 10 μM dimethylsilapentanesulfonic acid. Aliquots of Mg^{2+} were added as solutions of $MgCl_2$. The resulting Mg^{2+} concentrations were 0, 0.2, 0.4, 0.8, 1.2, 2.0, 3.6, 7.4, 18, 40, 81, and 190 mM. The final protein and Mg^{2+} concentrations were determined by amino acid hydrolysis and atomic absorption spectrophotometry, respectively. At each titration point, pH was adjusted by microliter additions of 0.1 M HCl or KOH. The $(Ca^{2+})_2$-TR_1C sample consisted of 0.2 mM ^{15}N-labeled TR_1C in H_2O with 10% D_2O, 2 mM $CaCl_2$, 150 mM KCl, 100 μM NaN_3, and 10 μM dimethylsilapentanesulfonic acid at pH 7.5.

Amide ^1H and ^{15}N chemical shifts were followed using sensitivity-enhanced and gradient-selected two-dimensional HSQC spectra, recorded with spectral widths of 1600 and 7692 Hz, sampled over 256 and 2048 complex data points in the ^{15}N and ^1H dimension, respectively. Using 18 scans per t_1-increment and a relaxation delay of 1.5 s, the total experimental time was 3.5 h/spectrum. ^{15}N nuclei were decoupled during acquisition using the GARP-1 sequence (46). All NMR spectra were recorded on a Varian Unity Plus spectrometer at a ^1H frequency of 599.89 MHz. ^1H chemical shifts were referenced to dimethylsilapentanesulfonic acid at 0 ppm and ^{15}N chemical shifts indirectly via the ^1H frequency using the frequency ratio ($^{15}N/^1H$) of 0.101329118 (47).

Data Processing—Amide chemical shifts were measured in the HSQC spectra at different Mg^{2+} concentrations. The spectra were processed for either resolution or sensitivity, using Lorentzian-Gaussian or Lorentzian line-broadening window functions in ω_2, and Kaiser or sine squared window functions in ω_1. After zero filling in ω_1, the matrix size was 1024 × 512 real points.

Amide line widths were measured from HSQC spectra processed using a Lorentzian line-broadening window function in both dimensions and zero-filling to 1024 points in ω_1. The final matrix size was 1024 × 1024. NMR line widths were determined from the HSQC spectra using the in house curve fitting software CFIT.[3,4] Fitting was performed by minimizing the error squared sum between a one-dimensional slice taken through the peak center and a pure Lorentzian line shape, as exemplified for Gly^{33} HN in Fig. 2. The Levenberg-Marquardt algorithm (48) was used, and starting parameters were obtained through an automatic search procedure.

Assignments—Sequential assignments of ^1H and ^{15}N resonances for $(Mg^{2+})_2$-TR_1C were obtained following standard procedures (49, 50), using the FELIX 95 software (MSI Inc.), GENXPK (51),[4] and the in house assignment tool ASSAR. The assignment procedure was facilitated by the close similarity of the chemical shifts to those of the ion-free state of intact CaM, kindly provided by Ad Bax. The complete ^1H and ^{15}N resonance assignments for $(Mg^{2+})_2$-TR_1C at 25 °C, pH 7.2, are deposited in BioMagResBank. ^1H and ^{15}N chemical shifts of ion-free TR_1C were assigned using the HSQC-TOCSY spectra and comparisons with the chemical shifts of ion-free intact CaM. Similarly, the Ca^{2+}-loaded form of the protein was assigned using the chemical shifts of Ca^{2+}-loaded intact CaM (52). The chemical shifts of the amide resonances in the HSQC spectra at different Mg^{2+} concentrations were assigned at increasing Mg^{2+} concentrations using the ion-free assignment and at decreasing Mg^{2+} concentrations using the $(Mg^{2+})_2$-TR_1C assignment.

Chemical Shifts—The binding kinetics of Mg^{2+} occur on the fast to intermediate NMR chemical shift time scale. Nuclei for which the

[2] P. Brodin, unpublished results.

[3] G. P. Gippert, unpublished results.

[4] Source code and instructions for GENXPK and CFIT are available on the World Wide Web at http://www.fkem2.lth.se/~garry/programs.html.

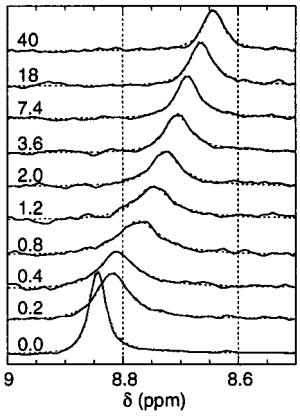

FIG. 2. **One-dimensional plots of the ^{1}H signal of Gly^{33} (*solid line*) and fitted curves (*dotted line*) at 0, 0.2, 0.4, 0.8, 1.2, 2.0, 3.6, 7.4, 18, and 40 mM $MgCl_2$, as indicated.**

chemical shift changes induced by Mg^{2+}-binding, $\Delta\delta$ (ppm), result in small resonance frequency changes compared with the exchange rate between two states, k_{ex}, are in the fast exchange regime; $2\pi\ \nu_0\ \Delta\delta \ll k_{ex}$, where ν_0 (MHz) is the spectrometer frequency of the nucleus observed. For these nuclei, the observed chemical shift is a population-weighted average of the shifts of the ion-free and Mg^{2+}-bound forms,

$$\delta = \delta_{\text{ion-free}} + \Delta\delta_{\text{I}}\, p_{\text{I}} + \Delta\delta_{\text{II}}\, p_{\text{II}} + \Delta\delta_{\text{I,II}}\, p_{\text{I,II}} \qquad \text{(Eq. 1)}$$

where p_{I}, p_{II}, and $p_{\text{I,II}}$ are the relative populations of the protein with an Mg^{2+} in site I, site II, and both site I and II, respectively, at a given Mg^{2+} concentration; $\delta_{\text{ion-free}}$ is the chemical shift of the ion-free state; and $\Delta\delta_{\text{I}}$, $\Delta\delta_{\text{II}}$, and $\Delta\delta_{\text{I,II}}$ are the chemical shift changes induced by Mg^{2+} binding to sites I, II, and both I and II, respectively. Nuclei experiencing resonance frequency changes of the same order of magnitude as the exchange rate ($2\pi\ \nu_0\ \Delta\delta \approx k_{ex}$) are in the intermediate exchange regime, where resonances are severely broadened by Mg^{2+} exchange. Their chemical shifts depend not only on the populations but also on the binding kinetics (53). Therefore, only resonances experiencing no or only moderate line broadening were used in the binding constant calculations.

Line Shapes—For a nucleus experiencing intermediate to fast exchange the contributions to the line width from the exchange process, $\Delta\nu_{1/2,\text{ex}}$, can be calculated as follows,

$$\Delta\nu_{1/2,\text{ex}} = \frac{4\pi\ \nu_0^2(\Delta\delta)^2 p_{\text{A}} p_{\text{B}}}{k_{\text{ex}}} \qquad \text{(Eq. 2)}$$

where

$$k_{\text{ex}} = k_{\text{on}}[Mg^{2+}] + k_{\text{off}} \qquad \text{(Eq. 3)}$$

and where p_{A} and p_{B} are the relative populations of the two states, k_{off} is the off-rate, k_{on} is the on-rate, and $[Mg^{2+}]$ is the free Mg^{2+} concentration. In the case where Mg^{2+} binding to a protein site is studied by adding Mg^{2+} to a given protein solution, the equation is readily rearranged to the following,

$$\Delta\nu_{1/2,\text{ex}} = \frac{4\pi\ \nu_0^2(\Delta\delta)^2}{k_{\text{off}}} \times \frac{K\,[Mg^{2+}]}{(1 + K\,[Mg^{2+}])^3} \qquad \text{(Eq. 4)}$$

where K is the binding constant to the site (54).

If line broadening is an effect of fast to intermediate conformational exchange *within* a certain state, the contribution to the total line width is approximately as follows,

$$\Delta\nu_{1/2,\text{ex}} = p\Delta\nu^0_{1/2} \qquad \text{(Eq. 5)}$$

where p is the relative population of the state and is the line width at 100% of that state, which may be calculated from Equation 2.

Due to the generally larger changes in resonance frequency, $\nu_0\,\Delta\delta$, for ^{1}H compared with ^{15}N, a larger number of ^{1}H resonances than ^{15}N resonances are broadened during the titration. Broadening in the ^{1}H dimension renders the evaluation of ^{15}N line widths uncertain. Therefore, ^{15}N line widths will generally not be discussed in this paper.

Mg^{2+} Binding Constants and Exchange Rates—Mg^{2+} binding constants were derived from chemical shifts and line widths using a simulated annealing algorithm similar to that used previously (33). In the present study, however, the binding constants were determined for individual residues, and the average was calculated. The microscopic binding constants of loop I and II (K_{I} and K_{II}) were determined from chemical shifts of 12 residues. The ion-free shifts, $\delta_{\text{ion-free}}$, were taken directly from the ^{15}N HSQC spectrum of the ion-free state. The two microscopic binding constants, K_{I} and K_{II}, and the chemical shift changes induced by binding an Mg^{2+} to loop I, II, and both loops, $\Delta\delta_{\text{I}}$, $\Delta\delta_{\text{II}}$ and $\Delta\delta_{\text{I,II}}$, were determined minimizing the following expression,

$$\chi^2 = \sum_i^n (\delta_{\text{ion-free}} + \Delta\delta_{\text{I}}\, p_{\text{I}}(i) + \Delta\delta_{\text{II}}\, p_{\text{II}}(i) + \Delta\delta_{\text{I,II}}\, p_{\text{I,II}}(i) - \delta_{\text{obs}}(i))^2 \qquad \text{(Eq. 6)}$$

where $p_{\text{I}}(i)$, $p_{\text{II}}(i)$ and $p_{\text{I, II}}(i)$ are the relative populations of the Mg^{2+} bound to loop I, II, and both I and II, respectively, calculated from the binding constants and the protein concentration, and $\delta_{\text{obs}}(i)$ is the observed chemical shift for the nucleus at Mg^{2+} concentration i. All of the nuclei chosen had a Mg^{2+}-induced chemical shift change of between 0.04 and 0.15 ppm for ^{1}H and 0.1 and 0.4 ppm for ^{15}N and showed no or only moderate broadening. The uncertainties were estimated as the maximal deviation causing a doubling of χ^2.

The microscopic binding constant of loop I (K_{I}) was also determined from line widths of six residues at or near this loop that experience moderate line broadening (5–20 Hz). K_{I}, the line width without exchange broadening before and after this binding event ($\nu_{1/2,\text{nat}}$), and the ratio of the squared Mg^{2+}-induced chemical shift change and the off-rate ($(\Delta\delta)^2/k_{\text{off}}$) were determined by minimizing the following expression,

$$\chi^2 = \sum_i^n \left(\nu_{1/2,\text{nat}} + \frac{4\pi\ \nu_0^2(\Delta\delta)^2}{k_{\text{off}}} \times \frac{K_{\text{I}}[Mg^{2+}]}{(1 + K_{\text{I}}[Mg^{2+}])^3} - \nu_{1/2,\text{obs}} \right)^2 \qquad \text{(Eq. 7)}$$

where $[Mg^{2+}]$ is the free Mg^{2+} concentration calculated from the fitted K_{I} and a fixed K_{II}, and $\nu_{1/2,\text{obs}}$ is the measured line width.

The rates of the dynamic processes in loop II were estimated from a comparison of experimental and calculated line shapes. A four-site exchange program, based on the Bloch-McConnell equations (55), was used in this analysis.

RESULTS AND DISCUSSION

Chemical shifts of backbone and side chain ^{1}H–^{15}N pairs were determined from HSQC spectra at 12 Mg^{2+} concentrations ranging from 0 to 190 mM, in 150 mM KCl at 25 °C, pH 7.5. The titration provides evidence for two binding events, both characterized by dissociation constants in the millimolar range. As shown in Fig. 3, the major chemical shift changes occur in or around the N-terminal parts of the Ca^{2+} binding loops. The chemical shift changes in these regions are very similar to the Ca^{2+}-induced changes, clearly identifying the location of the Mg^{2+} binding sites to the Ca^{2+} binding loops. The first binding event is characterized by effects that are intermediate on the chemical shift time scale; the amide signals of residues Asp^{20}—Ile^{27} in the N-terminal part of loop I become broadened beyond detection at intermediate Mg^{2+} concentrations, and a large number of other signals are significantly broadened (Figs. 4 and 5*b*). This exchange broadening can be attributed purely to binding to loop I, because all chemical shift changes of the same size do not result in the same degree of line broadening. When Mg^{2+} binds to loop II, no line width maxima appear at intermediate Mg^{2+} occupancies, but some signals are continuously broadened as the loop is filled (Fig. 5*c*). This indicates faster binding kinetics of this loop and a conformational exchange within the Mg^{2+}-bound form. Sequential binding of two Mg^{2+} is possible to demonstrate using the present method, because the two events are characterized by different degrees of exchange broadening and, for some signals, chemical shift changes of different signs, *cf.* Leu^{69} HN in Fig. 5*a*. At the highest Mg^{2+} concentration, a number of signals that are visible at lower salt concentrations become broadened beyond detection. This may be the result of changes in the time scale of the exchange processes within the $(Mg^{2+})_2$

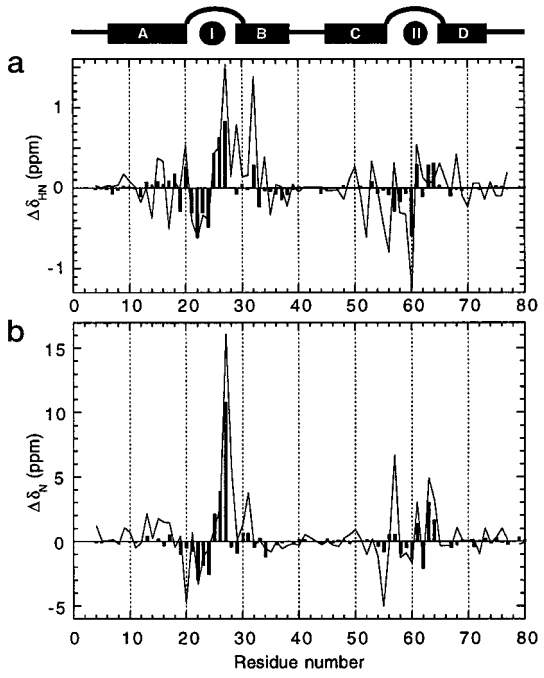

FIG. 3. **Backbone amide ^{1}H (*a*) and ^{15}N (*b*) chemical shift changes induced by binding two Mg^{2+} (*bars*) and two Ca^{2+} (*line*) to ion-free TR_1C as a function of residue number.** The concentrations were 81 mM $MgCl_2$ and 2 mM $CaCl_2$, respectively. The chemical shift effects of an increased ionic strength comparable with the added $MgCl_2$ are negligible on this scale.[5]

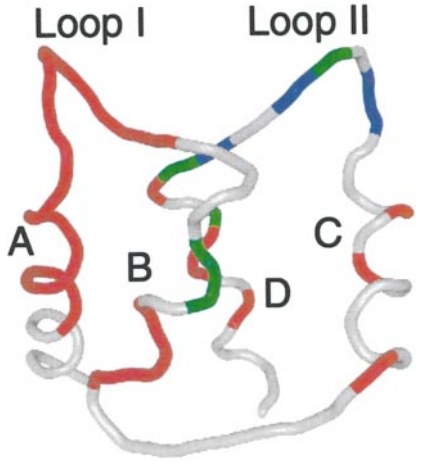

FIG. 4. **Backbone trace of the ion-free N-terminal domain of calmodulin (16).** Residues with protons experiencing significant exchange broadening during Mg^{2+} binding to loop I are colored *red*; those with protons experiencing significant exchange broadening due to conformational exchange in the Mg^{2+}-saturated loop II are colored *blue*; and those with protons subjected to both effects are colored *green*. The two loops and the four helices are labeled. This *figure* was generated using UCSF software Midas Plus (60).

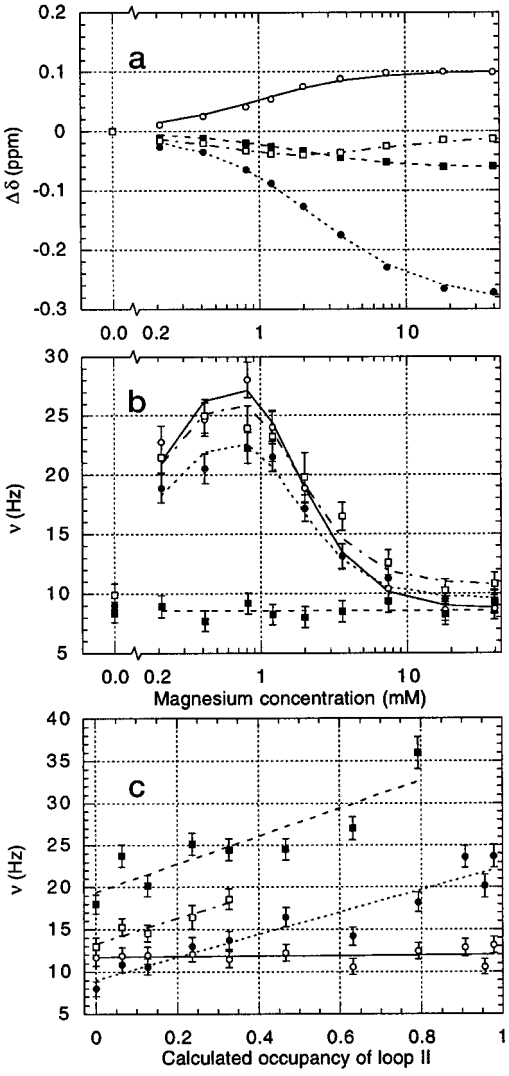

FIG. 5. **Titration curves of chemical shifts (*a*) and line widths (*b*) as a function of $MgCl_2$ concentration and line widths (*c*) as a function of calculated occupancy of loop II.** *Symbols* represent the measured values, with the *error bars* showing the uncertainty in the measurement, and *lines* represent fitted values. *a*, chemical shift fits are shown for Ser^{17} HN (*open circles*, *solid line*), Thr^{29} HN (*filled boxes*, *dashed line*), Ala^{57} HN (*filled circles*, *dotted line*), and Leu^{69} HN (*open boxes*, *dotted and dashed line*). *b*, line width fits are shown for Ser^{17} HN (*open circles*, *solid line*), Thr^{29} HN (*filled boxes*, *dashed line*), Val^{35} HN (*filled circles*, *dotted line*), and Leu^{69} HN (*open boxes*, *dotted and dashed line*). *c*, line width fits are shown for Ala^{57} HN (*filled circles*, *dotted line*), Gly^{59} HN (*open circles*, *solid line*), Gly^{61} HN (*filled boxes*, *dashed line*), and Ile^{63} HN (*open boxes*, *dotted and dashed line*).

state, nonspecific effects of the very high ionic strength, and/or transient aggregation.

Mg^{2+} Binding Constants—The microscopic Mg^{2+} binding constants (K_I and K_{II}) at high salt (150 mM KCl) for loops I and II in TR_1C were calculated using data exemplified in Fig. 5, *a* and *b*. K_I was calculated from the Mg^{2+}-induced line broadening (Fig. 5*b*), and K_I and K_{II} were calculated from the Mg^{2+}-induced chemical shift changes (Fig. 5*a*). The line shape calculations were based on the assumption that contributions to the signals included in the optimization from Mg^{2+} binding to loop II could be neglected. The chemical shift-based calculations were made using a number of different models, some including cooperative interactions. However, from the present data no additional information was obtained using more complicated models than a model with two independent binding loops. Binding constants obtained from chemical shifts and line shapes agree well. Since the precision of K_I was better using line shape analysis, this value was used to calculate K_{II} from the shift changes. The calculated microscopic Mg^{2+} binding constants are $\log_{10} K_I = 3.07 \pm 0.04$ and $\log_{10} K_{II} = 2.7 \pm 0.2$ (Table I). These values agree well with values obtained from Mg^{2+}/Ca^{2+} competition studies,[5] and earlier but less accurate determinations (24, 25). It is important to note that with such a small difference between the two binding constants, microscopic (K_I and K_{II}) and macroscopic (K_1 and K_2) binding constants are not equal ($K_1 = K_I + K_{II}$ and $K_2 = K_I K_{II}/(K_I + K_{II})$ under nonco-

[5] A. Malmendal, unpublished results.

TABLE I
Microscopic Mg^{2+} binding constants and off-rates of TR_1C

The microscopic binding constants and off-rates for Mg^{2+} in 150 mM KCl, at 25 °C, pH 7.5, were derived from amide ^1H and ^{15}N chemical shifts and ^1H line widths as a function of Mg^{2+} concentration.

	Loop I	Loop II
$\log_{10} K$	3.07 ± 0.04[a]	2.7 ± 0.2[b]
k_{off} (s^{-1})	380 ± 40[a]	~10,000[a]

[a] Determined from line shapes.
[b] Determined from chemical shifts.

operative conditions). The Mg^{2+} affinity is low compared with the Ca^{2+} affinity, but since the intracellular Mg^{2+} concentration is about 1 mM, the binding constants imply that almost 50% of the EF-hand loops in this domain will be occupied by Mg^{2+} at resting Ca^{2+} levels (Fig. 6).

$(Mg^{2+})_2$ TR_1C—Upon Ca^{2+} binding to CaM domains, the helix packing changes drastically (Fig. 1, *b* and *c*) (Refs. 16–18; see above). This major structural rearrangement is manifested in large backbone chemical shift changes, not only in the binding loops but also in the rearranging helices. The Mg^{2+}-induced backbone chemical shifts are more localized, with the larger changes appearing primarily in the N-terminal parts of the binding loops (Fig. 3). Relatively minor shift changes in the C-terminal parts of the loops in Mg^{2+} loaded TR_1C suggest that the Glu residues in the 12th position of the loops do not directly coordinate the smaller Mg^{2+}. The chemical shift changes in the N-terminal part of loop I are generally similar to those obtained upon Ca^{2+} binding. The differences indicate a slightly different accommodation by the ligands around the smaller Mg^{2+}. A plausible mode of Mg^{2+} coordination would be that observed in loop II of calbindin D_{9k}, where all Ca^{2+} ligands, except the bidentate Glu, also coordinate Mg^{2+} (32). In the case of loop I of TR_1C, a strikingly similar relation between the amide proton chemical shifts of the Mg^{2+}- and Ca^{2+}-loaded states of this loop and the same two states of loop II in calbindin D_{9k} corroborates this hypothesis. Such a mode of binding would explain why Mg^{2+} binding does not induce the same global structural rearrangements in the domain as Ca^{2+} binding does, and it further emphasizes the importance of the Glu in the 12th loop position. In the Mg^{2+}-loaded loop II, many resonances appear halfway between the chemical shifts of the ion-free and Ca^{2+}-loaded states (Fig. 3). This can be explained by a local rapid conformational exchange within the Mg^{2+}-loaded state of this site (see below).

Mg^{2+} Binding to Loop I, the Higher Affinity Site—During the first Mg^{2+}-binding event, the majority of signals from amide protons in the core of the N-terminal EF-hand are significantly broadened. The maximal line widths during this Mg^{2+} binding event are found at 0.8 mM added Mg^{2+} (Fig. 5*b*), and most signals have normal line widths above 18 mM (when loop I is 95% saturated). The observed line broadening is attributed to chemical exchange of Mg^{2+} in loop I. Assuming that the total amide proton chemical shift changes for residues Phe^{12}, Lys^{13}, Ala^{15}, and Ser^{17} in helix A originate entirely from this binding event, the off-rate is 380 ± 40 s^{-1} at 25 °C (Table I). On the same assumption, the absolute chemical shift changes associated with Mg^{2+} binding to loop I were estimated (Fig. 7). A number of signals from residues in helix C and helix D also experience significant line broadening (Figs. 4 and 7). In the structure of ion-free CaM (16, 17), many of them are in close proximity to the broadened residues in the N-terminal EF-hand (19). A significant number of these residues are located around the bidentate Ca^{2+} ligand Glu^{67} in the 12th position of loop II (Fig. 1*a*). At lower Mg^{2+} concentrations, this residue displays one of the most markedly broadened ^1H resonances outside of loop I, and it experiences large chemical shift

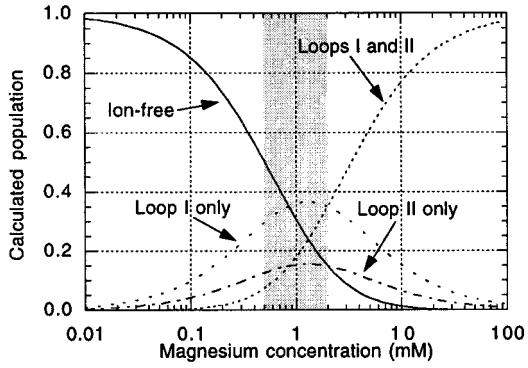

FIG. 6. **Calculated populations of the different states of TR_1C as a function of Mg^{2+} concentration.** The populations were calculated for $\log_{10} K_I = 3.07$, $\log_{10} K_{II} = 2.7$, and 1 μM protein. The *shaded area* represents the free Mg^{2+} concentration in eukaryotic cells.

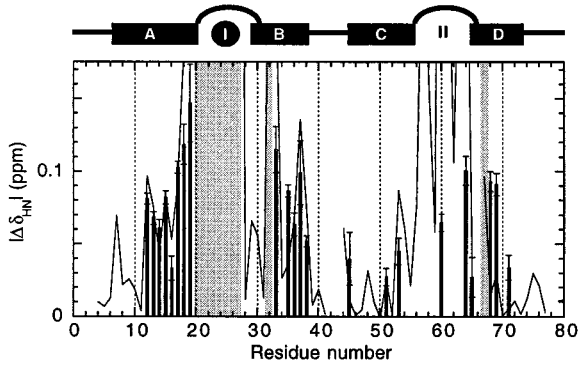

FIG. 7. **Absolute amide proton chemical shift changes induced by Mg^{2+} binding to loop I calculated from line width variations (*bars*) and the absolute value of the chemical shift change induced by binding of two Mg^{2+} (*line*; 81 mM $MgCl_2$), as a function of residue number.** The *shaded areas* represent residues showing significant broadening that were not quantifiable due to overlap and/or too extensive broadening.

changes of different signs due to the two binding events. The rearrangements necessary to accommodate Mg^{2+} in loop I may thus be transmitted through the hydrophobic core of the N-terminal EF-hand so as to reposition essential residues at the C-terminal end of loop II.

In the E140Q mutant of TR_2C, the bidentate Glu in the 12th position of the C-terminal loop IV is replaced by a Gln. Essentially, this mutant protein binds Ca^{2+} sequentially and does not seem to adopt the "open" conformation when only loop III is occupied by Ca^{2+} (33). The chemical shift changes induced by Ca^{2+} binding to loop III of this mutant protein are exceedingly similar in magnitude and location to those induced by Mg^{2+} binding to loop I of TR_1C, indicating that these two different ions have similar effects on the overall structure of the two different proteins. An interesting feature is that the C-terminal end of the occupied loop and the spatially close N-terminal end of the empty loop are much more affected by Ca^{2+} than Mg^{2+}. These different responses of the local environments may be explained by the different accommodation of the two ions: Mg^{2+} is ligated using only residues in the N-terminal part of loop I in $(Mg^{2+})_1$-TR_1C, while Ca^{2+} is ligated using also residues in the C-terminal part of loop III of $(Ca^{2+})_1$-E140Q-TR_2C. The antiparallel arrangement of the two loops, with coupling between the N-terminal half of one loop and the C-terminal half of the other and *vice versa*, provides a mechanism for cooperative Ca^{2+} binding. Since Mg^{2+} only binds to the N-terminal parts of the loops, it cannot employ this mechanism of cooperativity.

Mg^{2+} Binding to Loop II, the Lower Affinity Site—At the

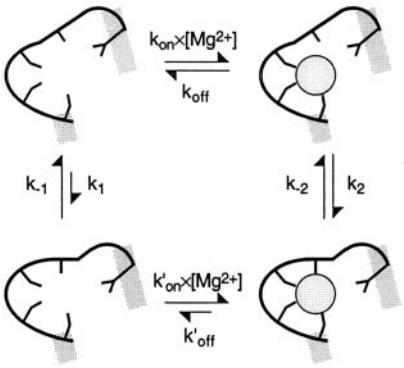

FIG. 8. **A four-site model of Mg^{2+} binding to loop II.** The state with an empty site is shown to the *left*, and the state with a filled site to the *right*. In each state, the "lower affinity conformation" is shown at the *top*, and the "higher affinity conformation" at the *bottom*. The empty "higher affinity conformation" is negligibly populated if $k_{-1} \gg k_1$ and $k'_{on} \times [Mg^{2+}] \gg k'_{off}$.

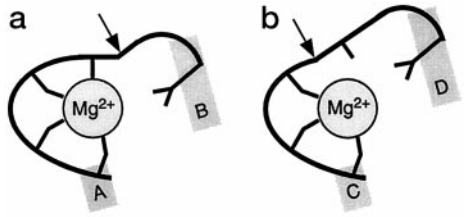

FIG. 9. **Schematic picture of loops I (*a*) and II (*b*) showing the localization of the hinge for the Ca^{2+}-induced structural rearrangements.** The four postulated Mg^{2+} ligands and the bidentate Ca^{2+} ligand are shown, the hinges are indicated by *arrows*, and the surrounding helices are indicated by *gray rectangles*.

second Mg^{2+} binding event, the major shift changes are located in loop II, where some signals (*e.g.* Ala^{57}, Asp^{58}, Asn^{60}, Gly^{61}, Ile^{63}, and Asp^{64} HN) are continuously broadened as $MgCl_2$ is added. At a first glance this broadening seems to be caused by Mg^{2+} exchange. However, in perspective of the calculated binding constants, implying loop II to be nearly saturated at the highest Mg^{2+} concentrations, these effects are more likely to be caused by exchange processes within the Mg^{2+}-loaded state.

When plotting the line broadening of residues in loop II *versus* the calculated degree of Mg^{2+} saturation of this loop, a linear dependence according to Equation 5 was obtained, as shown in Fig. 5*c*. According to Equation 2, the estimated line widths for a saturated loop II correlate well with the total Mg^{2+}-induced chemical shift changes for these residues, indicating exchange between a conformation similar to that in the ion-free state and a conformation optimizing the coordination of Mg^{2+}. Interestingly, the chemical shift changes of some amide signals in loop II are about 50% of those caused by Ca^{2+} binding (Fig. 3). The line broadening is interpreted assuming a four-state model with an empty and a Mg^{2+}-loaded state of the loop, each exchanging between a "low affinity conformation" and a "high affinity conformation" as shown in Fig. 8. If the chemical shift differences between the two conformations of the Mg^{2+}-loaded state is twice as large as the observed Mg^{2+}-induced shift changes, *i.e.* equal to the Ca^{2+}-induced shift changes for some residues, and if their populations are of equal magnitude, the exchange rate within this state would be ~10,000 s^{-1} at 25 °C. Similar exchange rates have been observed within Ca^{2+}-loaded states of TR_2C mutants (33, 34). If the population of the "high affinity conformation" is negligible in the absence of Mg^{2+} and the maximal chemical shift differences between the bound and unbound states of the "low affinity conformation" are of the same order as the maximal Mg^{2+}-induced chemical shift change for residues that do not show any line broadening during the titration (0.07 ppm), this model implies a lower limit for the Mg^{2+} off-rate from the "low affinity conformation" of the same order as the exchange within the Mg^{2+}-loaded state, *i.e.* ~10,000 s^{-1} at 25 °C. A slower off-rate would imply line width maxima at semisaturated states, as observed for binding to loop I. This value may be compared with the Mg^{2+} off-rate of ~3,000 s^{-1} at 25 °C and low ionic strength that was previously determined using ^{25}Mg NMR (25) under the assumption that the two Mg^{2+} exchange equally fast. With our present understanding of the slower Mg^{2+} exchange in loop I, the off-rate of the faster site can be recalculated as ~6,000 s^{-1}. Considering the difference in ionic strength, this is in good agreement with our present results.

Comparing the total Mg^{2+}-induced chemical shift changes with those calculated for the first binding event, the changes caused by the second event appear to be smaller. However, the signals in helices B, C, and D that experience chemical shift changes of different signs due to the two binding events show that also this binding event has effects all over the protein. Amide proton line widths of Leu^{32}, Gly^{33} (Fig. 2), Asn^{60}, Asp^{64}, and Glu^{67} are affected both by binding to loop I and the exchange process in loop II (Fig. 4) and experience line width minima at intermediate Mg^{2+} concentrations. The amides of Leu^{32} and Gly^{33} in helix B have an α-helical hydrogen bonding pattern in the Ca^{2+}-loaded state (15) but change this pattern due to a kink in the helix around Glu^{31} in the ion-free state (16, 17). This part of helix B may thus be structurally poorly defined in the Mg^{2+}-loaded states.

Mg^{2+} Accommodation in "Closed" EF-hands—The binding of ions of different sizes to EF-hands have been studied thoroughly (6, 7). Additional negative charges in the sites have been shown to increase the affinity for small ions less than for large ions (7). In the present case, the net charges of loop I and II are −3.8 and −4.4, respectively. If equal Ca^{2+} affinities of the two sites are assumed, stronger Mg^{2+} binding to loop I compared with loop II is successfully predicted. Drake *et al.* (56) have shown that in the EF-hand of *E. coli* galactose-binding protein the size and charge of the residue in the so called "gateway" position 9 of the loop is important for the binding kinetics. If this is the dominating determinant here, loop II should be the slower site. However, if the major structural rearrangements associated with Ca^{2+} coordination do not occur in the Mg^{2+} case, then the appearance of the CaM EF-hand sites may be so different that the "gateway" argument may not be applicable.

An important part of the Ca^{2+}-induced structural rearrangements in CaM take place around a hinge in the middle of the loops. This hinge is located asymmetrically in the two loops: between loop positions 8 and 9 at the end of the short β-sheet region in loop I and between loop positions 6 and 8 just before this β-sheet region in loop II (16) (Figs. 1 and 9). This has implications for the locations of the Ca^{2+} ligating backbone carbonyl oxygens in loop position 7, *i.e.* Thr^{26} and Thr^{62}, in the "closed" structure, which has not been subjected to the major Ca^{2+}-induced rearrangements. In Ca^{2+}-loaded CaM, the distances from Ca^{2+} to both of these oxygens are 2.3 Å (15). When the backbone atoms of the six N-terminal residues in loops I and II of the energy-minimized average structure of the ion-free state (16) are superimposed onto their respective counterparts in the Ca^{2+}-loaded state (root mean square deviation of 0.57 and 0.62 Å, respectively) the corresponding distance is still 2.3 Å for Thr^{26} but is 3.3 Å for Thr^{62}. This implies that the backbone conformation around Thr^{26} in loop I is suitable for Mg^{2+} ligation, while in loop II, the backbone carbonyl oxygen of Thr^{62} has to approach helix C in order to ligate Mg^{2+} (Fig. 9). The different levels of "preformation" of the two sites are probably reflected in the different Mg^{2+} affinities and Mg^{2+} binding

kinetics, with lower affinity, and faster kinetics in loop II. These features of loop II also support the hypothesis of exchange in the Mg^{2+}-loaded loop between a "high affinity conformation," providing a ligand geometry optimized for Mg^{2+}, and a relaxed "low affinity conformation" similar to the ion-free loop (Fig. 8).

An important residue in EF-hand loops is the conserved Gly in loop position 6, which allows the loop to make a sharp bend (12). A hydrogen bond between the amide proton of this Gly and a carboxylate oxygen of the Asp in the first loop position cause a downfield chemical shift of the amide proton (57, 58). In loops I and II, as in most EF-hand loops, these hydrogen bonds are strengthened upon Ca^{2+} binding (15–17). The chemical shift changes upon binding of two Mg^{2+} or two Ca^{2+} are virtually identical for the amide proton of Gly^{25} in loop I, showing the similarity of the N-terminal part of loop I when coordinating the two different ions. With this in mind, a Mg^{2+}-induced amide proton chemical shift change of Gly^{61} that is roughly 50% of that induced by Ca^{2+} binding and a continuous broadening of this signal upon Mg^{2+} saturation of loop II (Fig. 5*c*) favor the model with exchange between "high and low affinity conformations."

In a recent study (59), the ^{15}N chemical shift of Ile^{27} in position 8 of loop I was shown to depend on contributions of equal size from 1) polarization due to Ca^{2+} ligation by the preceding Thr^{26} backbone carbonyl oxygen and 2) changes in its side chain rotamer that are attributed to Ca^{2+} binding to loop II. At Mg^{2+} saturating conditions, the amide nitrogen of Ile^{27} has experienced a chemical shift change of 10.8 ppm compared with the Ca^{2+}-induced 16.1 ppm, and the signal is negligibly broadened. The line width at Mg^{2+} saturating conditions excludes chemical exchange at the rates observed for loop II between states with chemical shift differences comparable with the remaining 5.3 ppm and attributes the observed chemical shift to ligation by Thr^{26} only, with the difference compared with the Ca^{2+}-induced chemical shift explained by a lack of side chain rotation due to Mg^{2+} binding to loop II. The ^{15}N chemical shift of Ile^{63} in the same position of loop II does only depend on Ca^{2+} ligation by the preceding Thr^{62}, since the side chain rotamer is unaffected by Ca^{2+} binding. The Mg^{2+}-induced change is 3.0 ppm compared with 4.9 ppm induced by Ca^{2+}, and the signal is very broad at Mg^{2+} saturating conditions, which further supports the hypothesis of exchange between conformations with and without ligation by Thr^{62} in loop II.

To summarize, the $(Mg^{2+})_2$ state of TR_1C has the ions bound to the N-terminal part of the Ca^{2+}-binding loops in a manner similar to the $(Ca^{2+})_2$ state, but the overall conformation is "closed" as for the ion-free protein, since the smaller Mg^{2+} does not allow the side chain carboxylates of the Glu in the 12th loop position into the coordination sphere. The rearrangements in loop I are probably limited to the displacement of side chains to allow Mg^{2+} coordination. More significant side chain and backbone rearrangements in loop II are required to optimize coordination of Mg^{2+}, which result in the observed conformational exchange and a faster Mg^{2+} off-rate compared with loop I. The similar time scales observed for the conformational change and Mg^{2+} exchange suggest a coupling between the two events.

Conclusion—In a resting eukaryotic cell, the N-terminal domain of CaM is predicted to be almost half-saturated by Mg^{2+}. The protein does not exhibit the conformational rearrangements that occur upon Ca^{2+} binding, because coordination of the smaller Mg^{2+} involves only residues in the N-terminal part of the EF-hand loops, thus enabling the role of CaM as a specific mediator of Ca^{2+} signals. The different Mg^{2+} binding characteristics of the two loops reveal the asymmetry in the closed state of CaM. Ligands in loop I are better positioned for Mg^{2+} ligation, resulting in higher affinity and slower binding kinetics compared with loop II, in which exchange between a loop conformation optimizing the Mg^{2+} accommodation and a loop conformation more similar to that of the ion-free state is likely to occur. A relevant view of the N-terminal domain of CaM at resting Ca^{2+} levels may thus be that of a protein ensemble structurally similar to the ion-free protein but with significant populations of all of the half and fully Mg^{2+}-saturated states and with the dynamic behavior colored by a variety of Mg^{2+}-dependent effects.

Acknowledgments—We thank Drs. Mikael Akke, Göran Carlström, and Sara Linse for stimulating and fruitful discussions; Maria Selmer and Dr. Mikael Akke for valuable comments on the manuscript; and Dr. Ad Bax for the chemical shift assignments of ion-free CaM.

REFERENCES

1. Birch, N. J. (ed) (1993) *Magnesium and the Cell*, Academic Press Ltd., London
2. Cowan, J. (ed) (1995) *The Biological Chemistry of Magnesium.*, VCH publishers Inc., New York
3. Ebel, H., and Gunther, T. (1980) *J. Clin. Chem. Clin. Biochem.* **18,** 257–270
4. Evenäs, J., Malmendal, A., and Forsén, S. (1998) *Curr. Opin. Chem. Biol.* **2,** 293–302
5. Needham, J. V., Chen, T., and Falke, J. J. (1993) *Biochemistry* **32,** 3363–3367
6. Falke, J. J., Drake, S. K., Hazard, A. L., and Peersen, O. (1994) *Q. Rev. Biophys.* **27,** 219–290
7. Linse, S., and Forsén, S. (1995) in *Calcium Regulation of Cellular Function* (Means, A. R., ed) Vol. 30, pp. 89–152, Raven Press, New York
8. Tanokura, M., Imaizumi, M., and Yamada, K. (1986) *FEBS Lett.* **209,** 77–82
9. Kawasaki, H., and Kretsinger, R. H. (1994) *Protein Profile* **1**
10. Kretsinger, R. H., and Nockolds, C. E. (1973) *J. Biol. Chem.* **248,** 3313–3326
11. Henikoff, S., Greene, E. A., Pletrokovski, S., Bork, S., and Attwood, T. K. (1997) *Science* **278,** 609–614
12. Strynadka, N. C. J., and James, M. N. G. (1989) *Annu. Rev. Biochem.* **58,** 951–998
13. Linse, S., Helmersson, A., and Forsén, S. (1991) *J. Biol. Chem.* **266,** 8050–8054
14. Teleman, A., Drakenberg, T., and Forsén, S. (1986) *Biochim. Biophys. Acta* **873,** 204–213
15. Chattopadhyaya, R., Meador, W. E., Means, A. R., and Quiocho, F. A. (1992) *J. Mol. Biol.* **228,** 1177–1192
16. Kuboniwa, H., Tjandra, N., Grzesiek, S., Ren, H., Klee, C. B., and Bax, A. (1995) *Nat. Struct. Biol.* **2,** 768–776
17. Zhang, M., Tanaka, T., and Ikura, M. (1995) *Nat. Struct. Biol.* **2,** 758–767
18. Finn, B. E., Evenäs, J., Drakenberg, T., Waltho, J. P., Thulin, E., and Forsén, S. (1995) *Nat. Struct. Biol.* **2,** 777–783
19. Nelson, M., and Chazin, W. (1998) *Protein Sci.* **7,** 270–282
20. Finn, B. E., Drakenberg, T., and Forsén, S. (1993) *FEBS Lett.* **336,** 368–374
21. Bentrop, D., Bertini, I., Cremonini, M. A., Forsén, S., Luchinat, C., and Malmendal, A. (1997) *Biochemistry* **36,** 11605–11618
22. Drabikowski, W., Kuznicki, J., and Grabarek, Z. (1977) *Biochim. Biophys. Acta* **485,** 124–133
23. Walsh, M., Stevens, F. C., Kuznicki, J., and Drabikowski, W. (1977) *J. Biol. Chem.* **252,** 7440–7443
24. Drabikowski, W., Brzeska, H., and Venyaminov, S. Yu. (1982) *J. Biol. Chem.* **257,** 11584–11590
25. Tsai, M.-D., Drakenberg, T., Thulin, E., and Forsén, S. (1987) *Biochemistry* **26,** 3635–3643
26. Seamon, K. B. (1980) *Biochemistry* **19,** 207–215
27. Ohki, S., Ikura, M., and Zhang, M. (1997) *Biochemistry* **36,** 4309–4316
28. Ohki, S., Iwamoto, U., Aimoto, S., Yazawa, M., and Hikichi, K. (1993) *J. Biol. Chem.* **268,** 12388–12392
29. Chao, S.-H., Suzuki, Y., Zysk, J. R., and Cheung, W. Y. (1984) *Mol. Pharmacol.* **26,** 75–82
30. Declercq, J. P., Tinant, B., Parello, J., and Rambaud, J. (1991) *J. Mol. Biol.* **220,** 1017–1039
31. Houdusse, A., and Cohen, C. (1996) *Structure* **4,** 21–32
32. Andersson, M., Malmendal, A., Linse, S., Ivarsson, I., Forsén, S., and Svensson, L. A. (1997) *Protein Sci.* **6,** 1139–1147
33. Evenäs, J., Thulin, E., Malmendal, A., Forsén, S., and Carlström, G. (1997) *Biochemistry* **36,** 3448–3457
34. Evenäs, J., Malmendal, A., Thulin, E., Carlström, G., and Forsén, S. (1998) *Biochemistry* **37,** 13744–13754
35. Gagné, S. M., Li, M. X., and Sykes, B. D. (1997) *Biochemistry* **36,** 4386–4392
36. Brodin, P., Grundström, T., Hofmann, T., Drakenberg, T., Thulin, E., and Forsén, S. (1986) *Biochemistry* **25,** 5371–5377
37. Aue, W. P., Batholdi, E., and Ernst, R. R. (1976) *J. Chem. Phys.* **64,** 2229–2246
38. Wagner, G. (1983) *J. Magn. Reson.* **55,** 151–156
39. Braunschweiler, L., Bodenhausen, G., and Ernst, R. R. (1983) *Mol. Phys.* **48,** 535–560
40. Braunschweiler, L., and Ernst, R. R. (1983) *J. Magn. Reson.* **53,** 521–528
41. Bax, A., and Davis, D. G. (1985) *J. Magn. Reson.* **65,** 355–360
42. Cavanagh, J., and Rance, M. (1992) *J. Magn. Reson.* **96,** 670–678
43. Macura, S., and Ernst, R. R. (1980) *Mol. Phys.* **41,** 95–117
44. Zhang, O., Kay, L. E., Oliver, J. P., and Forman-Kay, J. D. (1994) *J. Biomol. NMR* **4,** 845–858

45. Grzesiek, S., and Bax, A. (1993) *J. Am. Chem. Soc.* **115,** 12593–12594
46. Shaka, A. J., Barker, P. B., and Freeman, R. (1985) *J. Magn. Reson.* **64,** 547–552
47. Wishart, D. S., Bigham, C. G., Yao, J., Abildgaard, F., Dyson, H., Oldfield, J., Markley, J. L., and Sykes, B. D. (1995) *J. Biomol. NMR* **6,** 135–140
48. Press, W. H., Flannery, B. P., Teukolsky, S. A., and Vetterling, W. T. (1986) *Numerical Recipes: The Art of Scientific Computing*, Cambridge University Press, Cambridge
49. Chazin, W. J., and Wright, P. E. (1988) *J. Mol. Biol.* **202,** 603–622
50. Wüthrich, K. (1986) *NMR of Proteins and Nucleic Acids*, John Wiley & Sons, Inc., New York
51. Gippert, G. P. (1995) *New Computational Methods for 3D NMR Data Analysis and Protein Structure Determination in High-dimensional Internal Coordinate Space.* Ph.D. thesis, The Scripps Research Institute, La Jolla, CA
52. Ikura, M., Kay, L. E., and Bax, A. (1990) *Biochemistry* **29,** 4659–4667
53. Sandström, J. (1982) *Dynamic NMR Spectroscopy*, 1st Ed., Academic Press, Inc., London
54. Campbell, I. D., and Dobson, C. M. (1979) *Methods Biochem. Anal.* **25,** 1–134
55. McConnell, H. M. (1958) *J. Chem. Phys.* **28,** 430–431
56. Drake, S. K., and Falke, J. J. (1996) *Biochemistry* **35,** 1753–1760
57. Ikura, M., Minowa, O., Yazawa, M., Yagi, K., and Hikachi, K. (1987) *FEBS Lett.* **219,** 17–21
58. Malmendal, A., Carlström, C., Hambraeus, L., Drakenberg, T., Forsén, S., and Akke, M. (1998) *Biochemistry* **37,** 2586–2595
59. Biekofsky, R. R., Martin, S. R., Browne, P., Bayley, P. M., and Feeney, J. (1998) *Biochemistry* **37,** 7617–7629
60. Ferrin, T. E., Huang, C. C., Jarvis, L. E., and Langridge, R. (1988) *J. Mol. Graphics* **6,** 13–27